Research Article Vol. 30, No. 6 / 14 Mar 2022 / Optics Express 9380
Optics EXPRESS

Multiband infrared emissions limited in the grazing angle from metal-dielectric-metal metamaterials

RIHAB BENLYAS, MAKOTO SHIMIZU,* KEIYA OTOMO, ZHEN LIU, AND HIROO YUGAMI

Department of Mechanical Systems Engineering, Graduate School of Engineering, Tohoku University, Aoba 6-6-01, Aoba-ku, Sendai 980-8579, Japan
makoto.shimizu.a3@tohoku.ac.jp

Abstract: Thermal radiation management remains a challenge because of the incoherent and isotropic nature of electromagnetic waves. In this study, a multiband and angular-selective infrared emitter, consisting of a simple one-dimensional (1D) metal-dielectric-metal metamaterial, is demonstrated. Although this structure has been well known as spectrally selective emitters, we analytically reveal that when the dielectric layer thickness is much smaller than the wavelength of interest (< 1/10), directive emission at nearly equal to the grazing angles (> 80°) can be obtained at multiple resonant wavelengths. As the absorption peaks can be entirely characterized by geometrical parameters, this angular selective technology offers flexible control of thermal radiation and can be adjusted to specific applications.

1. Introduction

Considering energy-saving issues, significant efforts have been devoted to controlling heat energy [1]. Thermal radiation, treated as isotropic and incoherent electromagnetic (EM) waves, remains difficult to shape. A strong and directional emissive power will enable novel applications, such as passive radiative cooling [2] and angular thermal emitters/absorbers [3] for solar thermophotovoltaics [4]. Spectral shaping has been studied thoroughly [1,5–10], whereas angular shaping remains challenging. With regard to angular dependence, a thin film of poly (methyl methacrylate) (PMMA) [11] was shown to exhibit highly angular-selective emission when the thickness becomes smaller than 500 nm. However, the narrowband emission and low thermal stability restrict the potential of this film as a thermal emitter.

An alternative would be plasmonic devices as the constituent material can withstand high temperatures. Although the potential for spectral shaping of plasmonic device was proven [5,12–18], angular dependency [19–22] has not attracted as much attention. In this context, angular-dependent phenomena such as critical-angle coupling epsilon-near-zero (ENZ) [23–28], and Berreman leaky modes (BLM) [4,23,25,29] are of particular interest. These polaritonic modes appear in thin subwavelength films, where the permittivity is close to zero. These modes appear at plasma frequencies for metals and at the longitudinal optical phonon frequencies for polar crystal films. Recently, relatively broadband (8 to 14 μm) emission and angular shaping is achieved through gradient ENZ structures in the far-infrared (IR) range [30]. However, the dependency on the intrinsic property of materials makes flexible multiband or broadband control of thermal radiation difficult. A possible solution is to design multiple resonances that would couple with these angular-dependent modes, which would produce a multiband and angular-selective emitter with a large emissivity at high angles.

Herein, we present a multiband and angular selective simple 1D metal-dielectric-metal (MDM) emitter based on couplings of surface plasmon polaritons (SPP) through gratings with leaky mode. The angular selectivity can be seen nearly equal to the grazing angle. As leaky mode

#450802 https://doi.org/10.1364/OE.450802
Journal © 2022 Received 8 Dec 2021; revised 6 Feb 2022; accepted 8 Feb 2022; published 8 Mar 2022

Optics EXPRESS

appears at the resonance, such as surface phonon or molecular vibrations, in the thin film on a reflective metal substrate [11,25], the aim is to couple it with multiple SPP resonances.

In fact, the MDM structure has been widely studied as a structure to obtain high absorption peaks due to the localized mode, which is generally recognized as an absorption (emission) mode with small angular dependence [31]. Although several papers reported the angular dependence of absorption intensity, [32,33], to the best of our knowledge, there are no reports of selective absorption or emission in the angular range close to grazing angle.

For a dielectric layer thickness that is much smaller than the wavelength of interest, the structure shows high angular-selectivity with multiple peaks throughout the IR range (in this study, from 3 to 10 μm by considering thermal radiation from 300°C materials), enabling the design of spectrum in angular-selective emitter. Using this technique, we believe that it will be possible to realize strong absorption/emission only at the limited direction over a wide range of wavelengths.

2. Design of the emitter

The structure consists of periodic gold gratings of 100 nm thickness with period P and width L deposited on a layer of SiO_2 of thickness d on top of a back reflective gold mirror, as shown in Fig. 1(a). Optical constant of each material is obtained from the handbook [34]. The rigorous coupled-wave analysis (RCWA) method (Rsoft, Diffract-MOD) was chosen to solve the Maxwell equations. A harmonic convergence study was conducted for every emitter with different dimensions. Assuming to apply the 300°C temperature range, the absorption and reflection coefficients are computed from 3 to 10 μm with a step of 0.01 μm and between 0 and 89° for both TM and TE polarizations. The normalized EM field is also computed for the resonant wavelengths under high angles. The emitter was illuminated through a transparent air medium (n_{air}= 1). In agreement with the Kirchhoff's law, where the emissivity ε and absorptivity α are equal; $\alpha(\lambda, \theta) = \varepsilon(\lambda, \theta)$ with λ and θ being respectively the vacuum wavelength and incident angle, absorption rather than emission is considered. A structure with dimensions P= 10 μm, L= 9 μm, and d= 0.1 μm is considered. The difference from the usual metamaterial with plasmonic structures is that the grating width on the dielectric layer is much large to cover 90% of surface and the dielectric thickness is relatively small compared with the wavelength of interest to be controlled. Figure 1(b) shows the simulated angular absorption. The peak intensity is stronger at high angles more than 80°. It is clear that multiple peaks confirm the multiband behaviors as expected. In this structure, three types of resonances can be observed: the surface phonon excitation [35], SPPs, and the resulting excitation of FP-like resonances [36]. The mechanism behind the broader peaks is explained by the coupling of SPP into FP-like resonances given by the following equations [37];

$$2L\beta + \varphi_r = 2m\pi \tag{1}$$

$$\varepsilon_{SiO_2} k_{gold} + \varepsilon_{gold} k_{SiO_2} \tanh\left(\frac{k_{SiO_2} d}{2}\right) = 0 \tag{2}$$

$$\beta^2 - \varepsilon_{SiO_2} k_0{}^2 = k_{SiO_2}{}^2 \tag{3}$$

$$\beta^2 - \varepsilon_{gold} k_0{}^2 = k_{gold}{}^2 \tag{4}$$

where φ_r is the phase shift of reflection, and L is the width of the grating, which represents the cavity length of this FP-like resonance mode. The wave vector and dielectric constant are expressed in k and ε, respectively, and the subscripts 0, SiO_2, and gold indicate the values in vacuum, SiO_2, and gold, respectively. The complex propagation constant of the SPP in an SiO_2 layer sandwiched by gold layers is expressed by β. In Eq. (1) corresponds to the FP-like mode resonance condition and Eq. (2) corresponds to the dispersion relation of propagation mode in an SiO_2 layer sandwiched by gold layers. Substituting Eq. (3) and (4) into the dispersion relation yields the propagation constant.

Optics EXPRESS

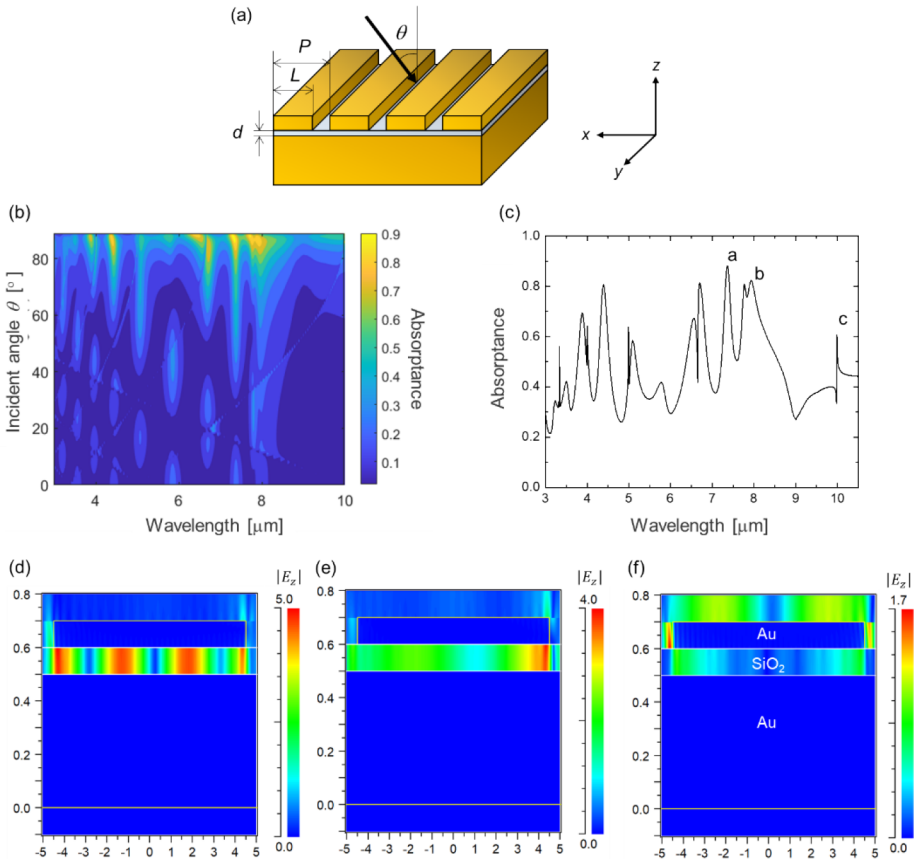

Fig. 1. (a) Geometry of the emitter(absorber) considered in this study. A thin SiO_2 layer with thickness of d is coated on the gold mirror. On top of the SiO_2 layer, a one-dimensional gold grating with period of P and width of L is formed. In the simulation, the thickness of the grating is constant to be 0.1 μm. The incidence is from a direction perpendicular to the grating with a zenith angle of θ. (b) A contour map of the simulated absorptivity spectrum with different incident angle from 0° to 89° using the model with P= 10 μm, L = 9 μm, and d= 0.1 μm under TM irradiance. (c) Absorptance spectrum of this structure with incident angle of 85°. Intensity distribution of $|E_z|$with typical resonance mode; (d) FP-like mode (3rd mode), (e) SiO_2 surface phonon mode and (f) Surface plasmon polariton mode shown in (c) as indicated by a, b and c, respectively.

Comparing the position of the absorption peak wavelength in the simulation, the calculated values are in perfect agreement, confirming that the absorption peak is due to the coupling of the SPP to the FP-like resonance. The peak appeared at 7.9 μm corresponds to surface phonon mode of SiO_2, which is called as Berreman mode [25] and the sharp peaks at 10 μm, 5 μm, and 3.33 μm correspond to the SPP [38]. The positions of these peaks are in perfect agreement with the theory. The electric field amplitude in z-direction shown in Fig. 1(d)-(f) clearly show the origin of typical peak indicated as a, b and c in Fig. 1(c). In other words, the clear resonance mode attributed to the third-order confinement mode can be seen in Fig. 1(d), but no confinement mode is not observed in Fig. 1(e). The semicircular arc of electric field attributed to the surface plasmon polariton is appeared at the grating surface in Fig. 1(f).

The reason of large absorption only at grazing angle can be explained from three aspects. One of the explanations can be given based on the report from Todorov et al. [32]. They pointed out

Optics EXPRESS

the dipole moment in the x-direction due to the charge distribution of stripes with similar MDM structure. Their analysis showed that the resonance, what we call as FP-like resonance, with even modes show no peak at 0° incident light because the dipole moment is not generated due to the symmetry. Whereas as the incident angle of light increases, the symmetry is broken, and the absorption increases. This is also seen in our results. However, we still cannot explain why the absorption attributed to the odd modes and the SiO_2 surface phonon mode are particularly large at the grazing angle. To follow up this point, it can be explained by considering the following two effects as well. The x-direction dipole moment generated on the stripe by the FP-like mode, the surface phonon mode, and the surface plasmon polariton mode would induce dipole-moment on the surface of Au substrate. These modes can couple with leaky mode. As described in Ref. [11], since the leaky mode has momentum close to the light line, the light incident from grazing angle can be strongly absorbed by exciting resonance modes with the help of leaky mode. In addition, if we consider the MDM structure as a layered structure,0 the angular selectivity also comes from the phase matching condition. If the phase of incident light matches with that of the light through the structure, the incident light can go into the layered structure without loss. It can be clearly understood from the literature [38] that the phase difference becomes zero at a specific angle close to 90° by replacing the lossy thin films with transparent ones.

The ratio of the average absorptivity at 80° and 10° angles of incidence, expressing the angular selectivity, shows that it decreases with relative thickness according to the exponential function as shown in Fig. 2. Here, the relative thickness is defined as $d_r = d/(5\ \mu m)$. To use the 5 μm as the wavelength of interest is derived from the emission peak wavelength from 300°C blackbody which we aim to apply this technology. The angular selectivity shows 5.7 at a relative thickness of 0.002, while it is 2.9 at 0.1. The ratio of the average absorptivity represents the normalized increase of the absorptivity at an incident angle of 80 degrees. This clearly indicates that the increase in the absorptivity at grazing angle is associated with the leaky mode because the exponential decay of angular selectivity as increasing the SiO_2 thickness [39] indicate the contribution of evanescent wave. Red-shift occurs by reducing the film thickness, but it is not a large shift, so the improvement in angular selectivity does not depend on this.

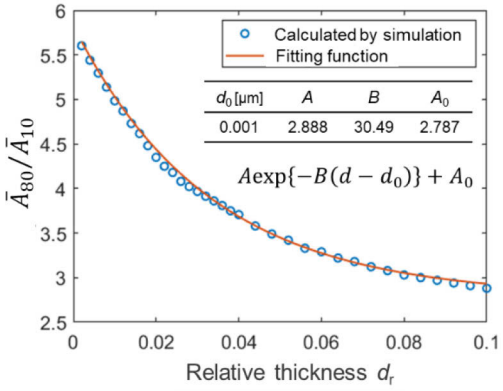

Fig. 2. The ratio of average absorptivity, from 3 to 10 μm, between incident angles of 80° and 10° as a function of relative thickness defined as $d_r = d/(5\ \mu m)$.

The polar plots of average absorptivity with L/P= 0.9 and thicknesses d of 0.03, 0.10 and 0.50 μm are shown in Fig. 3(a). Since the FP-like resonance modes are determined by width of the stripe, the width impacts the number of peaks. For larger width, more absorption peaks are observed as more FP-like resonance modes can be excited. Here, the MDM structure has L= 9

Optics EXPRESS

μm and P= 10 μm as similar to the Fig. 1. It can be also understood from these plots that the angular selectivity becomes larger as decreasing of the SiO_2 thickness.

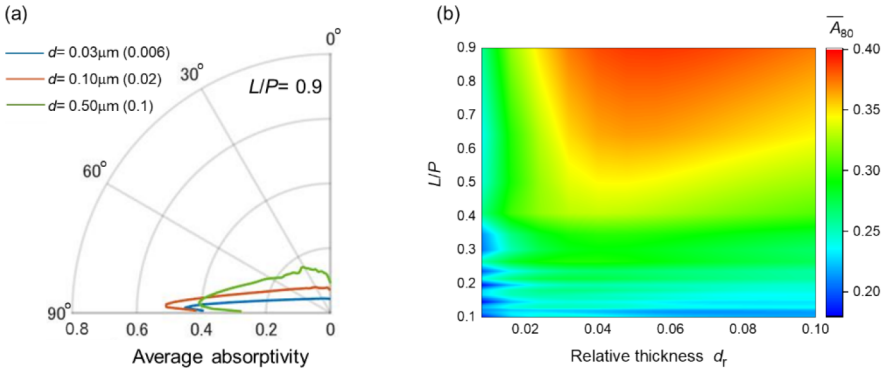

Fig. 3. (a) Simulation of the angular dependence of the average absorptivity from 3 to 10 μm using models with P= 10 μm and L= 9 μm. Three different SiO_2 thicknesses with d= 0.03, 0.10 and 0.50 μm are considered. The relative thicknesses are shown in parenthesis for each. (b) The average absorptivity at incident angle of 80° is simulated by varying L/P with fixing L as 9 μm and relative thicknesses.

In addition, L/P is affected to the intensity of the absorption peaks. As the fill factor increases to 0.9, the average absorptivity becomes 0.5. This value is 2.4 times larger than that of only SiO_2 film on the Au substrate. The large L/P is appropriate to enlarge the average absorptivity as described in Fig. 3(b). As such, the emitter is designed for large fill factors of at least 0.8, and the SiO_2 thickness is set at values around 0.1 μm, leading to a relative thickness of 0.02.

3. Experimental results and discussion

The emitter was fabricated using successive sputtering, laser lithography, and a lift-off process. First, the gold layer was sputtered on a silicon substrate using a radio frequency magnetron sputtering machine (Shibaura, CFS-4EPLL) at power of 300 W for gold and SiO_2, 100 W for chromium, and pressure of 0.5 Pa. The thickness of gold is 120 nm to eliminate the transmission. To improve the adhesion of gold on the silicon substrate, 5 nm of chromium was introudced. Then, approximately 5 nm of chromium was sputtered again followed by the layer of SiO_2 of variable thicknesses. The thickness was measured using a stylus profilometer (SURRCORDER ET200). The samples were then prepared for laser lithography. First, the adhesion promoter Hexa-Methyl-Di-Silazane (HMDS) was spin coated for 20 s at 3000 rpm followed by soft baking for 5 min at 115°C. The negative resist (ZPN 1150, Zeon) was then spin coated for 20 s at 3000 rpm. The sample was then baked at 90°C for 90 s. A mask less aligner (MLA150, Heidelberg instruments) was used for direct laser lithography. The sample was exposed to a dose of 200 mJ/cm^2. Post-exposure baking was then performed at 105°C for approximately 60 s. The sample was then developed using tetramethylammonium hydroxide (TMAH 2.38%) for about 50 to 60 s with vigorous shaking. Then, approximately 5 nm of chromium and 100 nm of gold were sputtered. The thickness of the sputtered chromium was small enough to have a negligible impact on the experiment, according to the simulation results. Finally, the resist was lifted off using the resist stripper 1-Methyl-2-pyrrolidon (NMP). For clean lift-off, the sample was immersed in an NMP solution at 80 °C for 5 h. The remaining resist was removed in an ultrasonic bath in the NMP solution for 5 min. The samples were then rinsed with isopropanol and distilled water.

As shown in Fig. 4(a), the gratings with the dimensions of P= 10 μm, L= 9 μm are fabricated as expected. SiO_2 layer thickness is measured during the fabrication and verified that the thickness is

Optics EXPRESS

almost 0.1 μm. The normal reflectance R_0 of the emitter is measured through FT-IR spectroscopy (FTIR-6300, JASCO), with attachments for both 10° and 80° angles. A polarizer is used to study the dependence on polarization. The absorptivity is then calculated by A= 1-R_0 owing to the presence of the bottom gold layer, which eliminates the transmission. The FT-IR equipment was used with attachments for R_0 measurements at different angles. The attachments were used to measure the specular reflectance at 10° (RF-81S, JASCO) and at 80° (RAS PRO410-B, JASCO). The various angle attachment (PR-510i, JASCO) was used to measure from 55° to 83°. A wire grid polarizer (KRS-5, JASCO) was used to evaluate the reflectance with TE and TM polarization. The measurement is conducted in a nitrogen gas atmosphere to reduce gas absorptions.

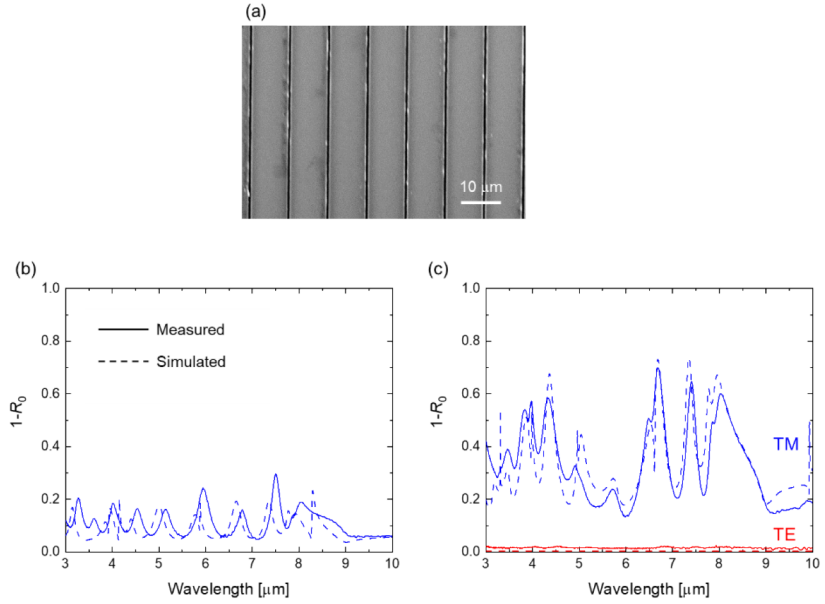

Fig. 4. (a) A top view SEM image and (b) measured absorptivity with θ= 10° and (c) θ= 80° of the fabricated structure with P = 10 μm, L = 9 μm, and d = 0.11 μm. The solid lines show the measured results obtained by 1-R_0 and the dashed lines show the simulated ones.

Regardless of the angle of incidence, in the case of TE-polarization, the absorptivity is as low as that of a gold mirror, as in the simulation (see Fig. 4(c)). For TM-polarization, the multiple peaks are observed, and both of the spectra are coherent with the simulation. The slight differences are due to small difference between the simulation model and the experiment, and also with the experimental SPP being of lower quality than that of the ideal simulated model. Indeed, in the experiment, the sharp peaks are broader and lower in intensity, merging with nearby peaks. The angular selectivity is very clear through the increase of the number of peaks and absorptivity at the high angle of 80° as opposed to the low angle of 10°. As can be seen in Fig. S1 in Supplement 1, globally, the absorptivity remains relatively low up to an angle of 80° and keeps increasing, then the intensity shows the highest for the angle of 83°, the maximum angle measurable by our instrument. These results are coherent with the simulation and confirm the angular selectivity of this structure.

To experimentally evaluate the influence of the thickness of the SiO_2 layer on the angular selectivity, the absorption enhancement factor $\bar{A}_{80}/\bar{A}_{10}$ is calculated from measured results in three samples with different SiO_2 thickness, as shown in Fig. 5. A comparison between the measured and simulated spectra are shown in Supplement 1 (see Fig. S2). In order to calculate the absorptivity directly, the hemispherical reflectivity including the diffracted light is necessary.

Optics EXPRESS

However, since it is difficult to evaluate the hemispherical reflectivity for high angle incidence, the absorptivity is estimated by measuring the normal reflectivity in this study because the diffraction effect is small when the SiO_2 layer is very thin. Thus, absorptivity is almost rightly evaluated when the SiO_2 layer is very thin in the measurement.

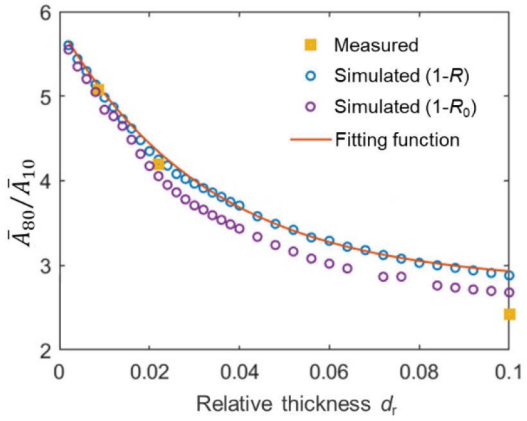

Fig. 5. Experimental result of the ratio of average absorptivity, from 3 to 10 μm, between incident angles of 80° and 10° as a function of relative thickness defined as $d_r = d/(5\,\mu m)$. The calculated $\bar{A}_{80}/\bar{A}_{10}$ from measured results are shown as yellow plots, and from simulated total absorptivity and corresponding fitting function are respectively in blue circle plots and a red line. The purple circle plots are the calculation from simulated normal reflectivity.

As the thickness of the SiO_2 layer increases, the effect of diffraction increases and the difference between hemispherical reflectivity and normal reflectivity becomes larger (see Fig. S3 in Supplement 1). This is the reason that the absorption enhancement factor $\bar{A}_{80}/\bar{A}_{10}$ calculated from the simulated normal reflectivity is also plotted in Fig. 5, and the decreasing trend of the measured $\bar{A}_{80}/\bar{A}_{10}$ is closer to the purple plots. For the largest relative thickness d_r of 0.10 in the experiment, where the diffraction effect is the strongest, the enhancement is slightly smaller than that in the simulation. Nevertheless, the general decreasing trend in the absorption enhancement factor as the SiO_2 thickness increases is consistent with the theory, and the angular selectivity is proven to appear for sufficiently small dielectric layer thicknesses.

The presented technology provides a new and simple method for thermal radiation management from both angular selectivity and spectral controllability. In addition, since the device is fabricated using successive sputtering and direct laser lithography, it is less expensive than plasmonic devices that use more complex geometries.

This structure emits thermal radiation directionally toward high angles, thus providing an efficient remote heat transfer method for distant objects whose view factor is small for usual isotropic emission. For example, when we assume a 1×1 cm emission surface and surrounding walls which have 0.5 cm height, which is 2 cm away from the emission surface center as shown in Supplement 1, only 5% of the emission to the total emission is reached in the case of the isotropic emission. Whereas 48% is reached using the proposed angular selective thermal emitter. The analysis results with the other geometry are shown in Table S1 in Supplement 1. The multiple bands throughout the IR range make it a flexible device for various applications at different temperatures. The peaks can be entirely characterized by the geometrical parameters, leading to flexible control of the thermal radiation. This addresses the material limitations often encountered with angular selective emitter originated from leaky mode, which depend on the material intrinsic resonance frequencies.

Optics EXPRESS

Gold is used as the main plasmonic material in this structure because we thought its high-quality resonance, resistance to corrosion, and high reflectivity are essential for the FP-like resonance. Nevertheless, similar angular selective property can be seen using other materials, such as titanium. The use of lossy materials leads to broadening of the peaks, which offers the possibility of realizing an all-broadband angular-selective emitter in the IR range, as can be seen in Fig. S4 in Supplement 1. The study conducted on 1D structures would be expanded to 2D emitters if the azimuthal angle dependence wants to be eliminated.

4. Conclusions

We have reported a multiband and angular selective emitter (absorber) based on the leaky mode excited by the coupling of SPP into FP-like resonances. This has been confirmed from exponential decays of the angular selectivity depends on the relative thickness, both from the simulation and the experiment. The average absorptivity more than 0.5, from 3 to 10 μm, can be obtained for the TM-polarized light incident from direction perpendicular to the grating with $\theta = 85°$. The average absorptivity in the peak angle will be higher by structure optimization because the absorption peaks can be entirely characterized by the geometrical parameters.

The presented technology is expected to contribute to the development of a new field of thermal radiation management by utilizing characteristics, i.e., flexible control of the spectral property and angular selective property, that are completely different from natural thermal radiation.

Funding. Japan Society for the Promotion of Science (JSPS KAKENHI Grant Number JP21K04894).

Acknowledgments. Part of this work was carried out in the Micro System Integration Center. The authors thank P.-O. Chapuis, O. Merchiers and Y. Kanamori for discussions.

Disclosures. The authors declare no conflicts of interest.

Data availability. Data underlying the results presented in this paper are not publicly available at this time but may be obtained from the authors upon reasonable request.

Supplemental document. See Supplement 1 for supporting content.

References

1. W. Li and S. Fan, "Nanophotonic control of thermal radiation for energy applications," Opt. Express **26**(12), 15995 (2018).
2. B. Bhatia, A. Leroy, Y. Shen, L. Zhao, M. Gianello, D. Li, T. Gu, J. Hu, M. Soljačić, and E. N. Wang, "Passive directional sub-ambient daytime radiative cooling," Nat. Commun. **9**(1), 5001 (2018).
3. W. L. Huang, H. H. Hsiao, M. R. Tang, and S. C. Lee, "Triple-wavelength infrared plasmonic thermal emitter using hybrid dielectric materials in periodic arrangement," Appl. Phys. Lett. **109**(6), 063107 (2016).
4. E. Sakr and P. Bermel, "Thermophotovoltaics with spectral and angular selective doped-oxide thermal emitters," Opt. Express **25**(20), A880 (2017).
5. C. Zhang, C. Huang, M. Pu, J. Song, Z. Zhao, X. Wu, and X. Luo, "Dual-band wide-angle metamaterial perfect absorber based on the combination of localized surface plasmon resonance and Helmholtz resonance," Sci. Rep. **7**(1), 5652 (2017).
6. M. Shimizu, K. Konno, F. Iguchi, and H. Yugami, "Fabrication of quasi-periodic surface microcavities by selective etching of self-organized superalloys for high-temperature photonics," Appl. Phys. Lett. **101**(22), 221901 (2012).
7. A. Kohiyama, M. Shimizu, F. Iguchi, and H. Yugami, "Narrowband thermal radiation from closed-end microcavities," J. Appl. Phys. **118**(13), 133102 (2015).
8. X. Liu, T. Tyler, T. Starr, A. F. Starr, N. M. Jokerst, and W. J. Padilla, "Taming the blackbody with infrared metamaterials as selective thermal emitters," Phys. Rev. Lett. **107**(4), 045901 (2011).
9. H. Zhang, F. Ling, and B. Zhang, "Broadband tunable terahertz metamaterial absorber based on vanadium dioxide and Fabry-Perot cavity," Opt. Mater. **112**, 110803 (2021).
10. M. Shimizu, M. Suzuki, F. Iguchi, and H. Yugami, "High spectral selectivity for solar absorbers using a monolayer transparent conductive oxide coated on a metal substrate," J. Appl. Phys. **121**(18), 183103 (2017).
11. S. Tsuda, S. Yamaguchi, Y. Kanamori, and H. Yugami, "Spectral and angular shaping of infrared radiation in a polymer resonator with molecular vibrational modes," Opt. Express **26**(6), 6899 (2018).
12. H. Zhu, F. Yi, and E. Cubukcu, "Plasmonic metamaterial absorber for broadband manipulation of mechanical resonances," Nat. Photonics **10**(11), 709–714 (2016).
13. C. Argyropoulos, K. Q. Le, N. Mattiucci, G. D'Aguanno, and A. Alù, "Broadband absorbers and selective emitters based on plasmonic Brewster metasurfaces," Phys. Rev. **87**(20), 205112 (2013).

Optics EXPRESS

14. C.-H. Fann, J. Zhang, M. ElKabbash, W. R. Donaldson, E. M. Campbell, and C. Guo, "Broadband infrared plasmonic metamaterial absorber with multipronged absorption mechanisms," Opt. Express **27**(20), 27917 (2019).
15. H. Lin, B. C. P. Sturmberg, K. T. Lin, Y. Yang, X. Zheng, T. K. Chong, C. M. de Sterke, and B. Jia, "A 90-nm-thick graphene metamaterial for strong and extremely broadband absorption of unpolarized light," Nat. Photonics **13**(4), 270–276 (2019).
16. T. Sang, J. Gao, X. Yin, H. Qi, L. Wang, and H. Jiao, "Angle-Insensitive Broadband Absorption Enhancement of Graphene Using a Multi-Grooved Metasurface," Nanoscale Res. Lett. **14**(1), 105 (2019).
17. L. P. Wang and Z. M. Zhang, "Resonance transmission or absorption in deep gratings explained by magnetic polaritons," Appl. Phys. Lett **95**(11), 111904 (2009).
18. Y.-H. Ye, Y.-W. Jiang, M.-W. Tsai, Y.-T. Chang, C.-Y. Chen, D.-C. Tzuang, Y.-T. Wu, and S.-C. Lee, "Coupling of surface plasmons between two silver films in a Ag/SiO_2 /Ag plasmonic thermal emitter with grating structure," Appl. Phys. Lett. **93**(26), 263106 (2008).
19. Y. Hwang and J. K. Yang, "Directional coupling of surface plasmon polaritons at complementary split-ring resonators," Sci. Rep. **9**(1), 7348 (2019).
20. D. M. Nguyen, D. Lee, and J. Rho, "Control of light absorbance using plasmonic grating based perfect absorber at visible and near-infrared wavelengths," Sci. Rep. **7**(1), 2611 (2017).
21. Y. L. Jing, Z. F. Li, Q. Li, P. P. Chen, X. H. Zhou, H. Wang, N. Li, and W. Lu, "Angular dependence of optical modes in metal-insulator-metal coupled quantum well infrared photodetector," AIP Adv. **6**(4), 045205 (2016).
22. L. Zhu, F. Liu, H. Lin, J. Hu, Z. Yu, X. Wang, and S. Fan, "Angle-selective perfect absorption with two-dimensional materials," Light: Sci. Appl. **5**(3), e16052 (2016).
23. W. D. Newman, C. L. Cortes, J. Atkinson, S. Pramanik, R. G. DeCorby, and Z. Jacob, "Ferrell-berreman modes in plasmonic epsilon-near-zero media," ACS Photonics **2**(1), 2–7 (2015).
24. S. Campione, F. Marquier, J.-P. Hugonin, A. R. Ellis, J. F. Klem, M. B. Sinclair, and T. S. Luk, "Directional and monochromatic thermal emitter from epsilon-near-zero conditions in semiconductor hyperbolic metamaterials," Sci. Rep. **6**(1), 34746 (2016).
25. S. Vassant, J.-P. Hugonin, F. Marquier, and J.-J. Greffet, "Berreman mode and epsilon near zero mode," Opt. Express **20**(21), 23971 (2012).
26. M. Habib, D. Briukhanova, N. Das, B. C. Yildiz, and H. Caglayan, "Controlling the plasmon resonance via epsilon-near-zero multilayer metamaterials," Nanophotonics. **9**, 3637 (2020).
27. N. C. Passler, I. Razdolski, D. S. Katzer, D. F. Storm, J. D. Caldwell, M. Wolf, and A. Paarmann, "Second Harmonic Generation from Phononic Epsilon-Near-Zero Berreman Modes in Ultrathin Polar Crystal Films," ACS Photonics **6**(6), 1365–1371 (2019).
28. S. Molesky, C. J. Dewalt, and Z. Jacob, "High temperature epsilon-near-zero and epsilon-near-pole metamaterial emitters for thermophotovoltaics," Opt. Express **21**(S1), A96 (2013).
29. I. Khan, Z. Fang, M. Palei, J. Lu, L. Nordin, E. L. Simmons, O. Dominguez, S. M. Islam, H. G. Xing, D. Jena, V. A. Podolskiy, D. Wasserman, and A. J. Hoffman, "Engineering the Berreman mode in mid-infrared polar Materials," Opt. Express **28**(19), 28590 (2020).
30. J. Xu, J. Mandal, and A. P. Raman, "Broadband directional control of thermal emission," Science **372**(6540), 393–397 (2021).
31. Y. Cai, Y. Huang, K. Zhu, and H. Wu, "Direction-independent dual-band perfect absorption induced by fundamental magnetic polaritons," Opt. Express **27**(20), A1431 (2019).
32. Y. Todorov, L. Tosetto, J. Teissier, A. M. Andrews, P. Klang, R. Colombelli, I. Sagnes, G. Strasser, and C. Sirtori, "Optical properties of metal-dielectric-metal microcavities in the THz frequency range," Opt. Express **18**(13), 13886 (2010).
33. Y. B. Chen and F. C. Chiu, "Trapping mid-infrared rays in a lossy film with the Berreman mode, epsilon near zero mode, and magnetic polaritons," Opt. Express **21**(18), 20771 (2013).
34. E. D. Palik, "*Handbook of Optical Constants of Solids*", Academic Press Inc., Orland (1985).
35. M. K. Gunde, "Vibrational modes in amorphous silicon dioxide," Physica B **292**(3-4), 286–295 (2000).
36. X. Liu, J. Gao, H. Yang, X. Wang, S. Tian, and C. Guo, "Hybrid Plasmonic Modes in Multilayer Trench Grating Structures," Adv. Opt. Mater. **5**(22), 1700496 (2017).
37. Y. Lee, K. Hoshino, A. Alù, and X. Zhang, "Tunable directive radiation of surface-plasmon diffraction gratings," Opt. Express **21**(3), 2748 (2013).
38. J. Park, J.-H. Kang, A. P. Vasudev, D. T. Schoen, H. Kim, E. Hasman, and M. L. Brongersma, "Omnidirectional Near-Unity Absorption in an Ultrathin Planar Semiconductor Layer on a Metal Substrate," Proc. SPIE **1**(9), 812–821 (2014).
39. B. Mario, S. Concita, and M. G. Angela, "*Evanescent Waves in Optics: An Introduction to Plasmonics*", Springer, NY (2017).